

# Differential Attention-Augmented BiomedCLIP with Asymmetric Focal Optimization for Imbalanced Multi-Label Video Capsule Endoscopy Classification

Podakanti Satyajith Chary <sup>a</sup>, Nagarajan Ganapathy <sup>b</sup>

<sup>a</sup> Department of Engineering Science, IIT Hyderabad <sup>b</sup> Department of Biomedical Engineering, IIT Hyderabad

Corresponding Author Email: [es25resch11002@iith.ac.in](mailto:es25resch11002@iith.ac.in)

Team Name: MINDH Lab

GitHub Repository Link:

[https://github.com/Satyajithchary/MINDH\\_ICPR\\_RARE-VISION\\_Challenge\\_2026](https://github.com/Satyajithchary/MINDH_ICPR_RARE-VISION_Challenge_2026)

## Abstract

This work presents a multi-label classification framework for video capsule endoscopy (VCE) that addresses the extreme class imbalance inherent in the Galar dataset [1] through a combination of architectural and optimization-level strategies. Our approach modifies BiomedCLIP [2], a biomedical vision-language foundation model, by replacing its standard multi-head self-attention with a differential attention mechanism [3] that computes the difference between two softmax attention maps to suppress attention noise. To counteract the skewed label distribution, where pathological findings constitute less than 0.1% of all annotated frames, a sqrt-frequency weighted sampler, asymmetric focal loss [4], mixup regularization [5], and per-class threshold optimization are employed. Temporal coherence is enforced through median-filter smoothing and gap merging prior to event-level JSON generation. On the held-out RARE-VISION test set comprising three NaviCam examinations (161,025 frames), the pipeline achieves an overall temporal mAP@0.5 of 0.2456 and mAP@0.95 of 0.2353, with total inference completed in approximately 8.6 minutes on a single GPU.

## 1 Motivation

Gastrointestinal (GI) disorders represent a significant global health burden, with conditions ranging from inflammatory bowel disease to gastrointestinal bleeding affecting millions of individuals annually. Video capsule endoscopy (VCE) offers a non-invasive means of visualizing the entire GI tract, particularly the small intestine, which remains inaccessible to conventional endoscopic techniques [6]. A single VCE examination, however, generates on the order of 50,000–130,000 image frames, requiring gastroenterologists to review extensive video data to identify clinically relevant findings that may appear in

only a handful of frames. This manual review is both time-intensive and prone to observer fatigue.

The Galar dataset [1] exemplifies the statistical challenge: anatomical regions (namely stomach, small intestine, colon) dominate the frame distribution, whereas pathological findings namely active bleeding, angiectasia, erosion, and ulcer are exceedingly sparse. In the training partition of 60 videos ( $\sim 494,696$  sampled frames), labels such as *z-line* (3 positive frames), *mouth* (73 frames), and *active bleeding* (150 frames) exhibit positive-to-negative ratios exceeding 1:3,000. Standard cross-entropy optimization under this distribution leads to models that achieve high frame-level accuracy by trivially predicting the majority class while failing to detect clinically significant rare events. This phenomenon is well-documented in the medical imaging literature, where minority-class recall collapses despite ostensibly high aggregate performance.

The motivation is twofold: firstly, to investigate whether differential attention, a mechanism that explicitly cancels attention noise through subtraction of dual softmax maps can yield more discriminative visual representations for subtle mucosal pathologies; and secondly, to develop a class-imbalance strategy that operates at multiple levels of the pipeline (namely sampling, loss weighting, augmentation, and post-processing threshold calibration) to ensure that rare pathological events receive adequate gradient signal during optimization.

## 2 Methods

The proposed pipeline comprises four stages: (1) an imbalanced data pipeline with class-aware sampling and augmentation, (2) a differential multi-task architecture combining vision-language contrastive learning with supervised classification, (3) a composite optimization objective, and (4) temporal post-processing for event-level prediction. The architectural overview is illustrated in Figure 1.

### 2.1 Backbone: Differential BiomedCLIP

The BiomedCLIP [2] is adopted as the foundation model, which comprises a Vision Transformer (ViT-B/16) image encoder pretrained alongside a PubMedBERT [7] text encoder on 15 million biomedical image-text pairs extracted from PubMed Central. This pretraining regime endows the visual encoder with domain-specific representations for histopathological, radiological, and endoscopic imagery.

To enhance the model’s capacity for distinguishing subtle pathological features from visually similar healthy mucosa, the standard multi-head self-attention in all 12 transformer blocks are replaced with differential attention [3]. Concretely, for a given input  $\mathbf{X} \in \mathbb{R}^{N \times d}$ , the  $h$  attention heads are partitioned into two groups of  $h/2$  heads each, yielding query-key pairs  $(\mathbf{Q}_1, \mathbf{K}_1)$  and  $(\mathbf{Q}_2, \mathbf{K}_2)$ . The attention output is computed as:

$$\text{DiffAttn}(\mathbf{X}) = \left( \text{softmax} \left( \frac{\mathbf{Q}_1 \mathbf{K}_1^\top}{\sqrt{d_h}} \right) - \lambda \cdot \text{softmax} \left( \frac{\mathbf{Q}_2 \mathbf{K}_2^\top}{\sqrt{d_h}} \right) \right) \mathbf{V} \quad (1)$$

where  $\lambda = \text{mean}(\exp(\boldsymbol{\lambda}_{q_1}^\top \boldsymbol{\lambda}_{k_1}) - \exp(\boldsymbol{\lambda}_{q_2}^\top \boldsymbol{\lambda}_{k_2}) + \lambda_{\text{init}})$  is a learnable scalar initialized at  $\lambda_{\text{init}} = 0.8$ , and  $d_h$  denotes the per-head dimension. By subtracting the second atten-

tion distribution from the first, differential attention cancels common-mode noise patterns—namely uniform or low-rank attention maps that arise when query-key similarity is uninformative—thereby amplifying signal from rare but diagnostically meaningful spatial regions.

Critically, pretrained weights from BiomedCLIP are fully transferred to the differential blocks. The fused QKV projection  $\mathbf{W}_{qkv} \in \mathbb{R}^{3d \times d}$  is decomposed into separate  $\mathbf{W}_q$ ,  $\mathbf{W}_k$ ,  $\mathbf{W}_v$  projections, while MLP and LayerNorm parameters are copied directly. This preserves the biomedical visual knowledge acquired during pretraining while introducing the differential attention parameterization.

## 2.2 Classification Architecture

The 512-dimensional image features from the ViT encoder are processed through two parallel pathways:

**Classification path.** Image features pass through an Excitation Block inspired by Squeeze-and-Excitation Networks [8], which applies a channel-wise gating mechanism with reduction ratio  $r = 16$ :

$$\mathbf{x}_{\text{out}} = \text{BN}(\mathbf{x} \odot \sigma(\mathbf{W}_2 \cdot \text{ReLU}(\mathbf{W}_1 \mathbf{x}))) \quad (2)$$

where  $\mathbf{W}_1 \in \mathbb{R}^{(d/r) \times d}$ ,  $\mathbf{W}_2 \in \mathbb{R}^{d \times (d/r)}$ ,  $\sigma$  denotes the sigmoid function, and BN is batch normalization. The gated features are then projected to 17 class logits through a linear layer preceded by dropout ( $p = 0.4$ ).

**Contrastive path.** Normalized image features are matched against frozen text embeddings generated by the PubMedBERT text encoder from clinical prompts of the form “*a video capsule endoscopy image showing [label]*”. Contrastive logits are computed as

$$\mathbf{z}_{\text{con}} = (\mathbf{x} / \|\mathbf{x}\|) \cdot \mathbf{T}^\top \cdot \exp(\tau), \quad (3)$$

where  $\mathbf{T}$  contains the 17 text embeddings and  $\tau$  is a learnable temperature parameter clamped to  $\exp(\tau) \leq 100$  for numerical stability.

## 2.3 How was class imbalance handled?

Class imbalance was addressed through a coordinated multi-level strategy: (i) a sqrt-frequency weighted random sampler that assigns each frame a sampling weight proportional to  $1/\sqrt{f_c}$  where  $f_c$  is the frequency of its rarest active label, providing moderate oversampling of rare classes without the instability of linear inverse weighting; (ii) asymmetric focal loss [4] with  $\gamma_+ = 1$ ,  $\gamma_- = 4$  that aggressively down-weights easy negative predictions which dominate in imbalanced settings while preserving gradient flow for positive examples; and (iii) per-class threshold optimization on the validation set, searching from 0.05 for rare classes (support < 1% of the dataset) to maximize class-specific F1 scores.

## 2.4 Regularization

To mitigate overfitting on the training distribution a concern given the high ratio of common to rare frames several regularization mechanisms were applied. Mixup [5] with

$\alpha = 0.3$  linearly interpolates pairs of training images and their multi-label targets, which acts as a data-dependent regularizer encouraging smoother decision boundaries. Label smoothing [9] with  $\epsilon = 0.05$  prevents overconfident predictions by softening hard binary targets to  $[0.05, 0.95]$ . Exponential moving average (EMA) of model parameters with decay  $\beta = 0.999$  provides an ensembling effect over training iterations, and the EMA weights are used for all validation and test inference. Additionally, strong augmentation comprising random resized cropping (scale 0.7–1.0), color jitter, horizontal and vertical flips, random rotation ( $\pm 15^\circ$ ), and random erasing is applied during training.

## 2.5 Optimization

The model is optimized with AdamW ( $\beta_1 = 0.9$ ,  $\beta_2 = 0.999$ ) and a weight decay of  $5 \times 10^{-4}$ , using a OneCycleLR schedule with maximum learning rates of  $9 \times 10^{-5}$  for the backbone and  $3 \times 10^{-4}$  for the classification head. The total loss is:

$$\mathcal{L} = \mathcal{L}_{\text{cls}} + 0.4 \cdot \mathcal{L}_{\text{con}} \quad (4)$$

where  $\mathcal{L}_{\text{cls}}$  is the asymmetric focal loss with class-frequency-derived positive weights (clipped to  $[1, 100]$ ), and  $\mathcal{L}_{\text{con}}$  is the binary cross-entropy computed on contrastive logits with the same positive weights. Training is conducted for 5 epochs on a single NVIDIA RTX PRO 6000 96GB GPU with batch size 128, requiring approximately 3 hours. The random seed is fixed at 42 for reproducibility.

## 2.6 Temporal Post-Processing

Frame-level sigmoid outputs are converted to temporal event predictions through a three-stage pipeline. Firstly, per-class optimized thresholds (determined on the validation partition) are applied to binarize predictions. Secondly, a median filter with window size  $w = 7$  is applied independently per class along the temporal axis to suppress isolated false positives, followed by gap merging that fills gaps of  $\leq 5$  frames between same-class events reflecting the clinical expectation that pathological findings persist over contiguous frame sequences in VCE data. Thirdly, events shorter than 3 frames are removed, and the remaining predictions are formatted into the competition JSON schema.

# 3 Results

## 3.1 Competition Metrics

The temporal mAP values reported below were computed using the official RARE-VISION evaluation web application and sanity checker, without any modification.

Overall mAP @ 0.5 — **0.2456**

Overall mAP @ 0.95 — **0.2353**

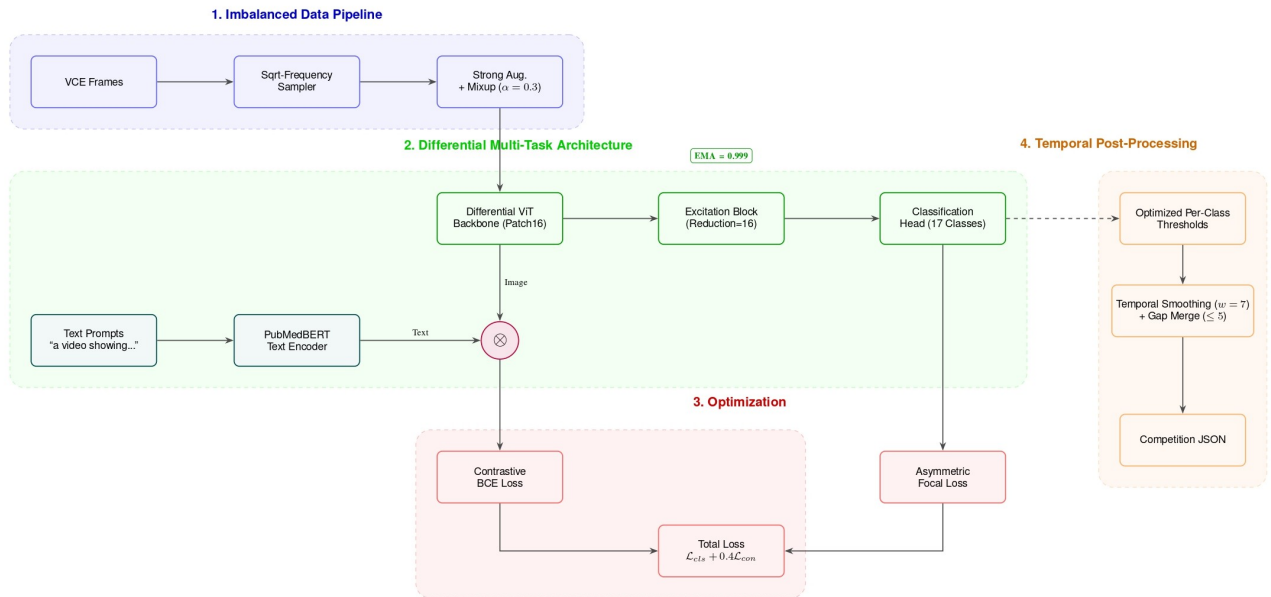


Figure 1: Overview of the proposed Differential BiomedCLIP pipeline. **Stage 1:** VCE frames are processed through a sqrt-frequency sampler and augmented with mixup ( $\alpha = 0.3$ ) and geometric/photometric transforms. **Stage 2:** The differential ViT backbone (Patch16, 12 blocks, 768-d) extracts 512-d image features, which are routed to both an excitation-gated classification head (17 classes) and a contrastive alignment module against PubMedBERT-encoded clinical text prompts. EMA ( $\beta = 0.999$ ) maintains a smoothed parameter copy. **Stage 3:** Asymmetric focal loss and contrastive BCE loss are combined as  $\mathcal{L}_{cls} + 0.4\mathcal{L}_{con}$ . **Stage 4:** Per-class optimized thresholds, temporal median smoothing ( $w = 7$ ), and gap merging ( $\leq 5$  frames) convert frame-level posteriors into the competition event JSON.

Table 1: Per-video temporal mAP on the RARE-VISION test set (3 NaviCam examinations).

Video ID	Frames	mAP@0.5	mAP@0.95
ukdd_navi_00051	44,878	0.2371	0.2353
ukdd_navi_00068	53,220	0.1808	0.1765
ukdd_navi_00076	62,927	0.3189	0.2941
<b>Average</b>	<b>161,025</b>	<b>0.2456</b>	<b>0.2353</b>

### 3.2 Validation Performance

On the validation partition (10 videos,  $\sim 80,399$  frames), the best checkpoint (epoch 4) achieved a frame-level macro-averaged AP of 0.2528. Table 2 presents the per-class breakdown. Anatomical regions with sufficient temporal continuity namely stomach (AP=0.849), small intestine (AP=0.969), and colon (AP=0.996) were classified with high precision. In contrast, rare pathological labels with extremely limited training support namely active bleeding (150 frames), erythema (232 frames), and hematin (2,565 frames) exhibited AP values below 0.03, reflecting the fundamental difficulty of learning discriminative representations from fewer than 0.05% of the training distribution.

Table 2: Per-class validation metrics at the best checkpoint (epoch 4). “Sup” denotes the number of positive frames in the validation set.

Label	AP	AUC	F1	Prec	Rec	Sup
mouth	0.244	0.991	0.267	0.261	0.273	22
esophagus	0.332	0.938	0.358	0.324	0.400	30
stomach	0.849	0.981	0.742	0.678	0.819	3,740
small intestine	0.969	0.989	0.847	0.743	0.986	20,608
colon	0.996	0.991	0.967	0.970	0.964	55,999
z-line	0.000	0.000	0.000	0.000	0.000	0
pylorus	0.006	0.593	0.069	0.077	0.063	16
ileocecal valve	0.001	0.322	0.014	0.020	0.010	98
active bleeding	0.002	0.522	0.000	0.000	0.000	100
angiectasia	0.028	0.932	0.011	0.008	0.020	51
blood	0.678	0.940	0.386	0.253	0.813	2,664
erosion	0.141	0.829	0.233	0.201	0.276	1,025
erythema	0.001	0.537	0.000	0.000	0.000	27
hematin	0.001	0.463	0.000	0.000	0.000	63
lymphangioectasis	0.011	0.696	0.029	0.017	0.084	119
polyp	0.026	0.729	0.007	0.018	0.004	928
ulcer	0.012	0.468	0.000	0.000	0.000	954
<b>Macro avg.</b>	<b>0.253</b>	<b>0.701</b>	<b>0.231</b>	<b>0.210</b>	<b>0.277</b>	—

### 3.3 Training Dynamics

The training loss decreased monotonically from 0.488 (epoch 1) to 0.176 (epoch 5), while validation loss rose moderately from 0.203 to 0.411 over the same interval. This controlled divergence (a factor of  $\sim 2.3\times$  at epoch 5) stands in contrast to preliminary experiments without regularization, where the validation loss exceeded the training loss by a factor exceeding  $15\times$  within 8 epochs. The OneCycleLR schedule decayed the learning rate from  $3 \times 10^{-4}$  to  $9 \times 10^{-8}$  over the 5-epoch budget. Validation mAP improved at every epoch (0.235, 0.239, 0.244, 0.253, 0.248), with the best checkpoint occurring at epoch 4.

### 3.4 Test Inference

Inference on the three NaviCam test videos (161,025 frames total) completed in 517.3 seconds (8.6 minutes) on a single NVIDIA RTX PRO 6000 GPU. Per-video inference times were 161.9s, 167.1s, and 188.3s for the 44,878, 53,220, and 62,927 frame videos respectively. The per-class optimized thresholds used for binarization ranged from 0.07 (hematin) to 0.83 (blood, angiectasia), reflecting the model’s calibration differences across the label frequency spectrum.

## 4 Discussion

The narrow gap between mAP@0.5 (0.2456) and mAP@0.95 (0.2353) across the test set indicates that the temporal boundaries of predicted events are well-localized when events are detected. This may be attributed to the median-filter smoothing and gap merging, which consolidate fragmented predictions into coherent temporal segments aligned with the continuous nature of capsule transit through the GI tract.

The per-video variance (mAP@0.5 ranging from 0.181 to 0.319) highlights examination. The strongest performance on `ukdd_navi_00076` (0.319) may correlate with the pathological distribution in that particular examination. Conversely, the weaker performance on `ukdd_navi_00068` (0.181) may reflect a higher proportion of ambiguous or overlapping pathological findings. Additionally, the test videos were acquired using the NaviCam system (480×480 pixels) whereas the majority of training data originated from Olympus Endocapsule (336×336 pixels) and PillCam (512×512 pixels) systems, introducing a domain shift in image resolution, color rendition, and field-of-view characteristics.

The principal limitation remains the rare pathological classes. Labels with fewer than 200 training frames (namely z-line, active bleeding, erythema, hematin) consistently exhibited AP below 0.01 despite sqrt-frequency oversampling and asymmetric focal loss. Morphologically, these conditions present as subtle mucosal changes for instance, angiectasia manifests as small, flat vascular ectasias that are visually indistinguishable from normal villi at low magnification, and erythema appears as diffuse reddening that overlaps substantially with the normal color variation of gastric and intestinal mucosa. The scarcity of training examples compounds this inherent visual ambiguity, as the model cannot build robust feature representations from the limited available signal. Future work may incorporate temporal modeling (namely recurrent or attention-based sequence modules) to leverage the sequential frame context, as pathological events in VCE data are characterized by temporal persistence and gradual morphological transitions that frame-level classifiers cannot exploit.

## 5 Summary

Team MINDH Lab utilized a Differential Attention-Augmented BiomedCLIP model, wherein the standard multi-head self-attention in all 12 ViT blocks was replaced with differential attention to suppress attention noise and amplify clinically meaningful visual features. A multi-level class imbalance strategy comprising sqrt-frequency weighted sampling, asymmetric focal loss ( $\gamma_- = 4$ ), label smoothing, mixup augmentation, and per-class threshold

optimization was utilized to handle class imbalance in the dataset. The narrow gap between mAP@0.5 and mAP@0.95 (0.0103 absolute difference) indicates precise temporal boundary localization attributable to the median-filter smoothing and gap-merging post-processing. The team achieved an overall mAP@0.5 of **0.2456**, and overall mAP@0.95 of **0.2353**.

## 6 Acknowledgments

As participants in the ICPR 2026 RARE-VISION Competition, we fully comply with the competition’s rules as outlined in [6]. Our AI model development is based exclusively on the datasets provided in the competition. BiomedCLIP [2], which is pretrained on publicly available PubMed Central data, was used as the foundation model as permitted by the competition rules. The mAP values are reported using the test dataset and sanity checker released in the competition. All code, model weights, and training logs (including loss curves and seed information) are available in the public GitHub repository.

## References

- [1] Maxime Le Floch, Franziska Wolf, Lara McIntyre, Christian Weinert, Alexander Palm, Kai Volk, Paul Herzog, Sven Holger Kirk, Jan Ludwig Steinhäuser, Claudia Stopp, et al. Galar—a large multi-label video capsule endoscopy dataset. *Scientific Data*, 12 (1):828, 2025.
- [2] Sheng Zhang, Yanbo Xu, Naoto Usuyama, Jaspreet Bagber, Robert Tinn, Sam Preston, Rajkumar Rajbhandari, Narun Song, and Hoifung Poon. BiomedCLIP: a multimodal biomedical foundation model pretrained from fifteen million scientific image-text pairs. *arXiv preprint arXiv:2303.00915*, 2023.
- [3] Tianzhu Ye, Li Li, Gao Huang, Sung Ju Hwang, Liwei He, and Peng Qi. Differential transformer. *arXiv preprint arXiv:2410.05258*, 2024.
- [4] Tal Ridnik, Emanuel Ben-Baruch, Nir Zamir, Asaf Noy, Itamar Friedman, Matan Protter, and Lih Zelnik-Manor. Asymmetric loss for multi-label classification. In *Proceedings of the IEEE/CVF International Conference on Computer Vision (ICCV)*, pages 82–91, 2021.
- [5] Hongyi Zhang, Moustapha Cisse, Yann N. Dauphin, and David Lopez-Paz. mixup: Beyond empirical risk minimization. In *International Conference on Learning Representations (ICLR)*, 2018.
- [6] Anni Lawniczak, Manas Dhir, Maxime Le Floch, Palak Handa, and Anastasios Koulaouzidis. ICPR 2026 RARE-VISION Competition Document and Flyer. 12 2025. doi: 10.6084/m9.figshare.30884858.v3. URL [https://figshare.com/articles/preprint/ICPR\\_2026\\_RARE-VISION\\_Competition\\_Document\\_and\\_Flyer/30884858](https://figshare.com/articles/preprint/ICPR_2026_RARE-VISION_Competition_Document_and_Flyer/30884858).

- [7] Yu Gu, Robert Tinn, Hao Cheng, Michael Lucas, Naoto Usuyama, Xiaodong Liu, Tristan Naumann, Jianfeng Gao, and Hoifung Poon. Domain-specific language model pretraining for biomedical natural language processing. *ACM Transactions on Computing for Healthcare*, 3(1):1–23, 2022.
- [8] Jie Hu, Li Shen, and Gang Sun. Squeeze-and-excitation networks. In *Proceedings of the IEEE/CVF Conference on Computer Vision and Pattern Recognition (CVPR)*, pages 7132–7141, 2018.
- [9] Christian Szegedy, Vincent Vanhoucke, Sergey Ioffe, Jon Shlens, and Zbigniew Wojna. Rethinking the inception architecture for computer vision. In *Proceedings of the IEEE/CVF Conference on Computer Vision and Pattern Recognition (CVPR)*, pages 2818–2826, 2016.